Hyperspectral remote sensing of planetary surfaces: an insight into composition of inner planets and small bodies in the solar system

Prakash Chauhan[1],*, Prabhjot Kaur[1], N. Srivastava[2], Rishitosh K. Sinha[2], Nirmala Jain[1] and S. V. S. Murty[2]

[1]Space Applications Centre, (ISRO), Ahmedabad 380 015, India
[2]Physical Research Laboratory, Ahmedabad 380 009, India

Space exploration missions of planetary bodies in our solar system have provided new insights to understand their formation and evolutionary processes that such bodies have undergone leading to their current geological state. Remote sensing from orbiter mission has helped in identifying surface features, delineating surface topography, mapping surface composition and deriving reliable age estimates of different planetary surfaces. In particular, high spatial and spectral resolution spacecraft observations have significantly contributed to our current understanding of the geological, physical and chemical processes that resulted in divergent evolutionary paths undertaken by different planetary objects such as inner and outer planets, dwarf planets, the moons and small solar system bodies (asteroids and comets). Hyperspectral remote sensing has been an emerging field of space-based reflectance spectroscopy and in recent years many imaging spectroscopy instruments have flown on different planetary missions, e.g. Moon Mineralogy Mapper on-board Chandrayaan-1, VIMS on Cassini mission, CRISM on Mars Reconnaissance Orbiter (MRO) mission, etc. This article provides a review on imaging reflectance spectroscopy for understanding the surface composition through mineralogy for different planetary bodies.

Keywords: Hyperspectral remote sensing, mineralogy, planetary surfaces, solar systems.

Introduction

EXPLORATION of planetary bodies is essential to understand their formation and decipher evolutionary processes leading to their current geological state. For distant and largely inaccessible planets, remote sensing, either from Earth-based telescopes or from a flyby/orbiter around the planetary body, as well as *in situ* probing by landers/rovers has efficiently helped in identifying surface features, delineating surface topography, mapping surface composition and deriving reliable age estimates. In particular, spacecraft observations have significantly contributed to our current understanding of the geological, physical and chemical processes that resulted in divergent evolutionary paths undertaken by different planetary objects such as inner and outer planets, dwarf planets, the moons and small solar system bodies.

The wide variety of planetary bodies in our solar system is reminiscent of the various stages of evolution that the solar system has undergone and detailed understanding about each of these is valuable to enhance knowledge about our own existence. Knowledge about factors governing their crustal structure and the evolutionary conditions may help in exploiting our own environment in a better way and also to explore possibilities for human settlement elsewhere[1]. Remote sensing studies in diverse fields like surface geology, atmosphere, geophysics, internal structure, seismology, etc. have contributed towards these aspects and have helped in developing suitable evolutionary models of planets. Many imaging spectroscopy instruments have flown on different planetary missions, e.g. Moon Mineralogy Mapper (M^3) on-board Chandrayaan-1, Visual and Infrared Mapping Spectrometer (VIMS) on Cassini mission, CRISM on Mars Reconnaissance Orbiter (MRO) mission, etc. The present article summarizes the role of hyperspectral imaging towards understanding the mineralogy of different planetary bodies.

The composition of minerals and their atomic structure reflect the physical and chemical conditions under which rocks have formed. Thus, mineralogical studies provide direct clues about key parameters, i.e. temperature, pressure, cooling rates, etc. of the associated rock types and hence help in reconstructing the geological environment that would have prevailed at the time of their formation[2]. Reflectance spectroscopy is a powerful tool for remote detection of minerals on the Earth and other planetary surfaces. It involves measurement of solar reflection from a target in the UV–VIS–NIR region of the electromagnetic spectrum in discrete spectral bands. The reflectance value plotted against wavelength produces a spectral reflectance curve, which exhibits characteristic features that

are used to identify the specific minerals present, thereby enabling identification of the rock types in an area.

The absorption features in the reflectance spectra are caused mainly due to electronic transitions and vibrational processes[3]. The presence of transition metal ions like Fe^{2+}, Fe^{3+}, Mg^{2+}, etc. in the atomic structure of minerals gives rise to electronic transitions in the near-infrared region (~ 0.7–2.6 μm) of the electromagnetic spectrum[3]. These transitions results in characteristic absorption features at particular wavelengths, which are peculiar to coordination geometry, atomic structure and composition of a mineral. Intensive research on visible–near-infrared (VNIR) reflectance spectroscopy of transition metal-bearing minerals during the past 40 years have resulted in volumes of literature detailing importance of the technique in identifying the minerals and deriving quantitative chemical estimates[4,5]. In comparison to the near-infrared region, the mid- and the thermal-infrared regions are dominated by the fundamental vibration of atoms present in the crystal lattice; generally water bearing minerals, salts and silicates[6]. In some minerals such as hydrated silica, phyllosilicates and sulphates, absorption also occurs at shorter wavelengths due to overtones or combinations of fundamental frequency[7].

Earth-based telescopes have been used for the collection of planetary spectral reflectance data during the early studies[8–10], which were limited by telescope availability, favourable observational conditions, coarse spatial resolution and optimum viewing alignment of the planetary objects. Further, prior to about 1990, satellite-based planetary remote spectroscopic measurements were limited to multispectral sensors which collect data in limited spectral bands from the visible and near-infrared region of the electromagnetic spectrum. Sampling of a spectral range of interest with a few broad channels only is the primary limiting factor of the multi-spectral sensor systems, which severely affects identification of mineral species and quantitative mineralogical assessment. Advances in sensor technology have overcome this limitation, with the development of satellite-based hyperspectral technology, or its variant known as imaging spectroscopy. A string of imaging spectrometers were flown to planetary missions, and as a result, at present, spectral reflectance data are available for a number of solar system bodies at a very high spatial and spectral resolution. Availability of these hyperspectral datasets in the VNIR range from orbiting/flyby missions has enabled global-scale compositional mapping of planetary bodies such as the Moon of the Earth, Mars, Saturn rings and Iapetus, the Moon of Saturn[11–24].

Reflectance spectroscopy for planetary composition

The reflectance spectra of most common rock-forming minerals are provided in Figure 1. Among these, olivine

and pyroxene are the most abundant minerals reported from the surfaces of Mercury[9], Venus[25], Earth and Moon[26], Mars[27], certain groups of asteroids[10,28] and meteorites[29]. Reflectance spectra of low-calcium pyroxenes (LCP) in the VNIR are characterized by two major absorption bands centred around 0.9 μm (band I) and 1.9 μm (band II) and are attributed to crystal field transitions in Fe^{2+} situated in the M2 crystallographic site. High-calcium pyroxene (HCP) spectra also show two absorptions; however, the bands are centred at slightly higher wavelengths, i.e. ~ 1.05 μm (band I) and 2.35 μm (band II)[3]. The primary absorption feature in olivine is a composite of three distinct absorption bands around 1 μm, which is attributed to the electronic transitions of Fe^{2+} occupying both the M1 and M2 crystallographic sites[3].

Water and OH (hydroxyl) produce three fundamental absorptions at 3.106, 6.079 and 2.903 μm in liquid phase; however, in water-bearing minerals the overtones of water can be observed at 1.4 μm and combinations of H–O–H bend with OH stretches are found near 1.9 μm (refs 6 and 30). In spectra of OH-bearing minerals, the absorption typically occurs near 2.7–2.8 μm, but can occur anywhere in the range from about 2.67 to 3.45 μm depending upon the ion to which it is attached[6,30]. Carbonates also show diagnostic vibrational absorptions with overtones and combinations that occur in the near-infrared region. The two stronger bands occur at around 2.50–2.55 and 2.30–2.35 μm and the three weaker ones occur near 2.12–2.16, 1.97–2.00 and 1.85–1.87 μm (refs 6 and 30).

Any planetary surface represents nonlinear mixtures and hence, the resulting spectra have contributions from the mixed surface materials occupying the Instantaneous Field of View (IFOV) of the sensor. For the sake of simplicity of interpretation, this mixing is often considered as linear; however, this approach has failed in numerous cases[31]. The other factors affecting the strength of absorption features in reflectance spectra include presence of opaques such as ilmenite, particle size and maturity due to space weathering[32–35]. With continued bombardment of the solar high-energy particles, galactic cosmic rays and micrometeorites on the lunar surface, agglutinates are formed and nano-phase reduced iron is deposited on the rims of mineral grains, which alter the composition dependent optical properties. This results in the weakness of characteristic absorption features, reduction in albedo and reddening of the continuum slope[32,33].

Hyperspectral sensors collect data in numerous, typically hundreds of narrow contiguous spectral bands producing detailed spectral reflectance data. Consequently, this allows extraction of accurate compositional information in comparison to the multispectral approach. The advent of hyperspectral technologies has led to multi-fold increase in the cost of the sensor/imager, data volumes to be stored and data-processing costs. Most of the hyperspectral sensors operate over the VNIR and SWIR region
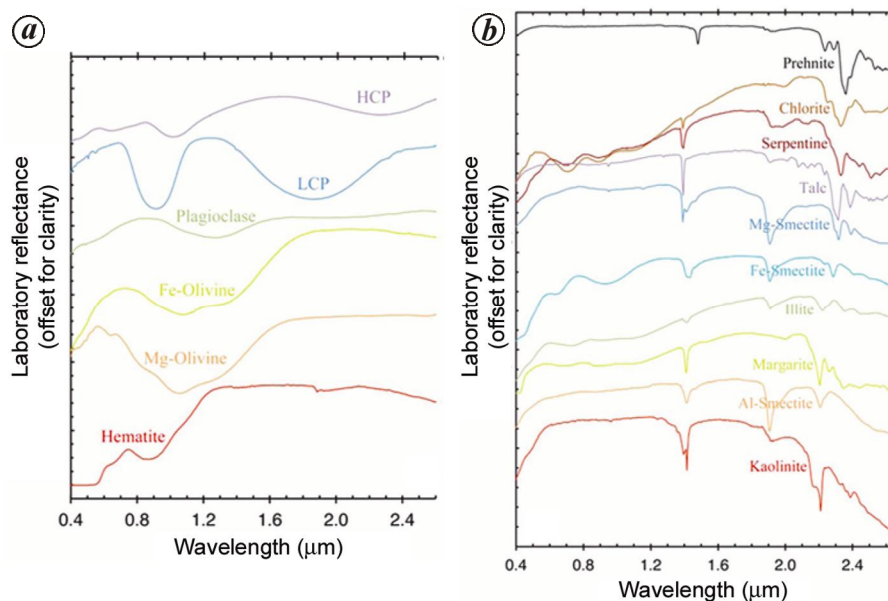
Figure 1. Reflectance spectra of (*a*) common rock forming minerals and (*b*) water-bearing minerals formed as alteration products on Mars. Figure adopted from Viviano-Beck *et al.*[34].

of the electromagnetic spectrum, exploiting solar illumination for detection and identification of materials on the basis of their reflectance spectra. As of now, many hyperspectral imaging spectrometers have orbited the Earth, Mars, Moon and Saturn. Table 1 provides a summary of the hyperspectral sensors flown on various planetary missions along with technical specification.

Lunar reflectance spectroscopy: historical perspective

Earth-based telescopic spectroscopy of the Moon started well before the Apollo astronauts landed on the Moon during late 60s and early 70s. The mare regions were mapped on the basis of albedo and absorption in the VNIR reflectance spectra[35–37]. Four compositionally sensitive spectral parameters – UV/VIS ratio, albedo, 1 μm band strength, and 2 μm band strength were used to distinguish Mare basalt types[35]. These studies established the distribution of volcanic materials across the lunar nearside and suggested that majority of spectrally distinct basalt types are not represented in the returned Apollo samples[35].

Multispectral imaging of the lunar surface started with Mariner 10 in 1970 and Galileo flybys in 1990, which provided the first opportunity to see and collect data from the western limb and far side of the Moon[38–40]. These areas were previously obscured from the Earth-based telescopic observations due to tidal locking of the Moon with the Earth. The year 1994 brought out upsurge in lunar science when NASA's Clementine mission provided the first global multispectral view of the entire Moon at a

spatial resolution as high as ~100 m. The UV–VIS imager onboard Clementine spacecraft had five bands, centred around 415, 750, 900, 950 and 1000 nm (ref. 41). The other multispectral imager for mineralogical studies was a near-infrared camera (NIR camera), which obtained images of nearly the entire lunar surface in six wavelengths: 1100, 1250, 1500, 1990, 2600 and 2700 nm (ref. 41). Despite having limited spectral coverage up to 1000 nm only, Clementine UV–VIS multispectral images provided unprecedented mineralogical details of the lunar surface on the basis of band strength, band position and shape of the band I absorption feature[42–45]. Clementine data, in combination with telescopic observations and laboratory measurements of Apollo returned samples, allowed developing methods for evaluating the chemical composition of the lunar surface. Data from these two sensors, especially the UV–VIS camera, were widely used to estimate TiO_2 and FeO content, maturity degree of the lunar surface and provided global maps for these[46–51].

In 1998, another mission Lunar Prospector of NASA orbited the Moon and provided accurate global chemical maps at a spatial resolution of ~150 m, mainly using γ-ray spectroscopy[51]. Data from Lunar Prospector gamma-ray spectrometer were utilized to study unique group high-alumina mare basalts which are derivatives of late-stage cumulates of Lunar Magma Ocean[52]. Other major findings include identification of geochemical anomalies on the far side of the Moon on the basis of thorium enhancement[53,54]. These inevitable findings helped in the renewal of lunar exploration and the cause of this was recognized as mentioned in the European Space Agency's report 'Europe's Priorities for the Scientific Exploration and Utilization of the

Table 1. Details of various hyperspectral instruments that orbited Moon, Mars and Saturn with their technical specifications

Planetary object	Instrument	Mission	Spectral range (µm) and no. of channels	Imaging/ non-imaging	Spatial resolution
Moon	Hyperspectral Imager (HySI)	Chandrayaan-1, ISRO	0.42–0.96, 64	Imaging	80 m
	Moon Mineralogical Mapper (M^3)		0.43–3.0, 85	Imaging	140 m/pixel from 100 km orbit
	Spectrometer Infrared (SIR-2)		0.9–2.4	Non-imaging, point spectrometer	220 m
	Spectral Profiler (SP)	Selene Kaguya, Japan	0.5–2.6, 296	Non-imaging	562 m × 400 m
Mars	Thermal Emission Spectrometer (TES)	Mars Global Surveyor (MGS)	5.8–50, 137	Non-imaging	3 × 6 km
	Observatoire pour la Minéralogie, l'Eau, les Glaces et l'Activité (OMEGA)	Mars Express, European Space Agency	0.36–5.2, 352	Imaging	0.3–4 km/pixel
	Compact Reconnaissance Imaging Spectrometer for Mars (CRISM)	Mars Reconnaissance Orbiter (MRO)	0.4–4.0, 554	Imaging	Global mode – 200 m/pixel targeted mode – 15–38 m/pixel
Saturn	Visual and Infrared Mapping Spectrometer (VIMS)	Cassini	0.35-5.1, 256	Imaging	500 µrad (nominal mode)

Moon' (ESA 1992) that resulted into a technological marvel, SMART-1 Moon mission of ESA (2003–2006). A string of missions from various space agencies followed SMART-1, which include Kaguya/SELENE of JAXA (2007), Chandrayaan-1 of ISRO (2008) and Lunar Reconnaissance Orbiter (LRO) of NASA (2009). Among these, SELENE and Chandrayaan-1 had hyperspectral spectrometers on-board for compositional mapping.

SELENE/Kaguya mission of Japan had both multispectral and hyperspectral sensors on-board Multi-band Imager (MI) and Spectral Profiler (SP) for lunar mineralogy studies[55,56]. SP is a non-imaging line-profiling spectrometer that worked in the VNIR range (500–2600 nm) with a footprint of 500 m × 500 m and acquired data in 162 spectral channels[55,56]. ISRO's Chandrayaan-1 spacecraft carried three hyperspectral sensors dedicated to mineralogical studies, namely, M^3 of NASA, Spectrometer Infrared (SIR-2) from Max-Planck Institute for Solar System Research, Germany, and Hyperspectral Imager (HySI) of ISRO. HySI worked in push-broom mode and mapped the lunar surface in 64 contiguous bands in the spectral range 0.42–0.96 µm (ref. 57 and 58). The SIR-2 instrument is a grating-based, compact, high-resolution, non-imaging point spectrometer operating in the 0.9–2.4 µm spectral range with a 6 nm spectral resolution[59]. M^3 is a push-broom hyperspectral imager which acquired lunar surface images at a resolution of 140 m/pixel in 85 contiguous spectral channels from 0.43 to 3.0 µm (ref. 60). All the three sensors discussed above produced a plethora of high-quality data, made available in the public domain, which were utilized by the scientific community all around the world, leading to many new discoveries.

New discoveries and results from recent lunar missions

Lunar magma ocean hypothesis explains the evolution of the lunar crust; therefore, investigation of the lunar crustal composition is crucial for validation of the hypothesis and understanding the progression of crystallization in the magma ocean[61]. Lithologies of central peak of widely distributed craters across the Moon using SP data led to the discovery[62] of crystalline iron-bearing pure plagioclase with an absorption feature around 1.3 µm, which confirmed the lunar magma ocean hypothesis. Also, in this study, previously identified olivine-rich exposures on the central peak of Tsiolkovsky crater using Clementine UV–VIS data[63] were interpreted as mixtures of plagioclase and pyroxene with the hyperspectral SP data. Another important discovery from SELENE data includes identification of possible mantle originated olivine exposures around some large impact basins on the lunar surface, which helped in understanding the global distribution and formation processes of these deposits[64]. The hyperspectral and imaging nature of M^3 facilitates full mineralogical characterization of the lunar surface, thus making it different from the other sensors. Several studies have been carried out using M^3 data, which provided important insights into the composition of the crust and deeper lithologies, compositional diversity at the central peak of the craters and characterization of spectrally distinct units within mare basins. Most importantly, M^3 data led to the discovery of widespread hydration feature across the lunar surface, as well as new rock type and played a vital role in the identification of neo-volcanic flows on the Moon. These findings have changed the view that the lunar surface is bone dry and geologically dead.

The new rock type revealed on the Moon using M^3 data is Mg-spinel anorthosite (devoid of mafic silicates) and is characterized by the presence of 2 µm absorption feature and lack of absorption at 1 µm (ref. 65). Subsequent to its discovery along the western rims of Moscoviense basin, this particular lithology, termed as pink spinel anorthosite (PSA), has been identified at several other locations on the lunar surface[66–71]. Most of the reported exposures are confined to the central peak of craters and rim of large basins/craters, which are understood to be composed of rocks exhumed from deeper crustal levels on the Moon due to megascopic meteoroidal impacts. The other surprising occurrence has been reported from Hansteen Alpha, a silicic dome situated in the Oceanus Procellarum area on the near side of the Moon[72].

Mg-spinels along mafic mineral assemblages known as OOS (olivine–orthopyroxene–spinel) have been reported along the inner basin ring of Moscoviense basin of the far side of the Moon[65]. The same OOS lithology has also been reported from the southern rim of the crater Endymion situated on the near side of the Moon[73]. The extent, distribution and mineralogical association of Mg-spinel dominant rocks identified from Orientale basin have indicated melt – wall rock reaction for their formation and suggested that extensive magmatism would have occurred in the region prior to the formation of the Orientale basin[74]. From the global occurrences of spinel-rich rocks reported from remote sensing studies, it has been inferred that Mg-suite magmatism may be quite widespread on the Moon and may not be just confined to the enigmatic Procellarum KREEP terrane, as thought earlier by many.

Another important study is the mineralogical characterization of the basalt flows within the various mare basins, which helps in understanding independent evolution of each mare basin and compositional behaviour of the source region. The central part of the Moscoviense basin situated on the far side of the Moon was studied to map the compositional units and establishment of the stratigraphic relationship between them using HySI data on-board Chandrayaan-1 (ref. 75). Despite the limited spectral coverage of the HySI sensor, the basin units have been mapped on the basis of slightly modified band parameters, i.e. band curvature, band tilt and band curvature, which were originally derived for Clementine data[45]. Another study includes compositional variability of the various basaltic flows within the Mare Serenitatis[15] (Figure 2).

Detailed spectral analyses have been carried out and pyroxene chemistry determined taking advantage of M^3 spectral range. The study brings out detailed information on the pyroxene variability within the various flow units of Serenitatis basin, which suggested that the source region of the basalt was quiet stable and did not experience large-sale fractionation[15]. The study of spectral characterization of basalts was extended to other young basalt flows (~1.2–2.8 Ga old) of the lunar surface as well,

such as in the Orientale basin and Mare Moscoviense[16]. The Moscoviense unit has been found to exhibit signatures of Fe-rich glasses and clinopyroxenes and the basalts of Orientale basin show distinct absence of olivine and are rich in HCP. Lithostratigraphic variations indicated that younger units of the Orientale basin and western nearside show distinctively higher FeO content compared to the older (immediate subsurface) basalt units. Further, it has been concluded that spectrally diverse volcanic activity occurred during similar time frame in widely separated regions of the Moon.

The spectral range of M^3 (~0.4–3.0 µm) enables detection and discrimination of olivine on the lunar surface on the basis of its characteristic 1 µm absorption and lack of 2 µm absorption, which was not possible with Clementine multispectral data. Compositional analysis of olivines is possible since the 1 µm absorption is a function of Mg number of olivine and shifts in a well characterized manner with changing Mg number (Mg#)[76]. Compositional analyses of lunar olivines have been made from some regions on the lunar surface which includes the northwest rim of the Moscoviense basin, central peak of the Copernicus crater, Aristarchus and Marius crater in the eastern Marius Hills[19]. The analysis includes continuum removal of the spectra, fitting of modified Gaussian model curves and prediction of composition in terms of Mg#. The forsteritic (high Mg#) composition is indicative of a primary source, whereas a more evolved source region is indicated by fayalitic (low Mg#) compositions[76]. The study showed the applicability of hyperspectral data in estimating the composition of lunar olivines remotely and thus, interpreting their geological significance.

M^3 used spectral information from the M^3 and DIVINER Lunar Radiometer on-board LRO for geochemical and mineralogical characterization of the Gruithuisen region on the Moon along with morphometric information[17]. Based on data analysis, silica saturated lithology has been delineated from silica under-saturated rocks, their spatial spread and non-mare nature of the Gruithuisen domes. It has been inferred that the three domes in the region (NW, γ and δ) would have tapped residual liquid from different parts of the magma chamber that was under constant mixing.

Another important significance of hyperspectral data in the field of mineralogy is the detection of glass deposits and separability from olivine and pyroxene mixture. The absorption features in reflectance spectrum of Fe-rich orange glass show absorption near 1 and 2 µm similar to pyroxene, but the bands are broader and the band I centre occurs at longer wavelength than a compositionally equivalent pyroxene. The Aristarchus crater was studied for discrimination of glass-rich deposits from olivine deposits using Spectral Angle Mapper (SAM) technique[77]. The same deposits have been verified using high-resolution panchromatic images from Terrain Mapping Camera (TMC) on-board Chandrayaan-1 and LROC NAC
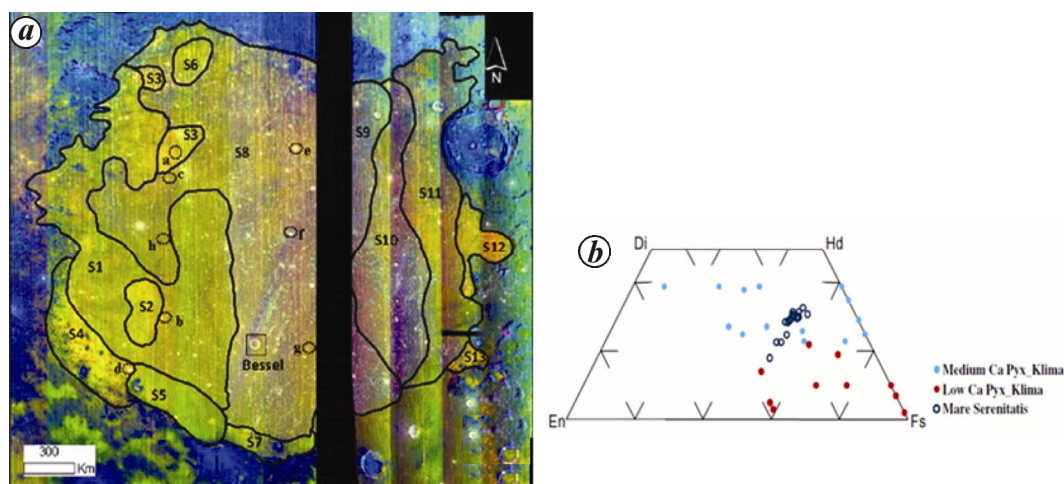
Figure 2. *a*, Mineralogical units of the Mare Serenitatis mapped using integrated band depth at 1 µm (red channel) and 2 µm (green channel) together with albedo at 1.58 µm (blue channel). *b*, Pyroxene quadrilateral plot showing pyroxene compositional range of Mare Serenitatis basalts plotted together with synthetic laboratory pyroxene data.

images from LRO mission. Compositional information derived using M^3 data for a young (2–10 million year old) volcanic formation inside Lowell crater, Orientale basin helped in differentiating the younger formation from the older impact melts present in the area[78,79].

One of the most remarkable discoveries from M^3 data from Chandrayaan-1 is the detection of adsorbed water and hydroxyl molecule on the lunar surface on the basis of absorption feature at 3 µm (ref. 80). The global data investigations reveal that the feature occurs systematically across the lunar surface, suggesting that the lunar surface contains primary hydrated minerals. The surficial process involving solar wind implantation of the H/OH molecules onto the lunar surface was suggested as the possible explanation for the observed hydration feature. The same hydration signature was also reported from the Compton–Belkovich volcanic complex (CBVC) situated on the far side of the Moon[81]. The study suggests that the enhanced hydration observed from CBVC is not surficial but may have originated during the episodic formation of the dome (Figure 3).

Similar hydration feature has been reported from Jackson crater associated with the fresh crystalline plagioclase slopes of the central peak and with pyroxene-rich walls of the crater[82]. Endogenic water has also been reported using M^3 data from the central peak of Bullialdus crater[83] and the Lowell crater region[78].

From the above discussions it can be concluded that hyperspectral imaging has vastly changed scientific perception about the Moon and has many applications for lunar mineralogy and has been used as a potential tool to resolve several geological mysteries of the Moon. Even though a large amount of information about the surficial water could be obtained using Chandryaan-1 hyperspectral data, the hydration features around 2.8–3.5 µm window could not be fully characterized due to limited

spectral range of M^3 data up to 3.0 µm. In order to extend these observations and to study the H_2O/OH formation processes on the Moon, a new hyperspectral sensor with wider spectral coverage (up to ~5 µm) is currently being developed at the Space Applications Centre (ISRO), Ahmedabad to be flown on Chandrayaan-2 mission.

Surface composition of Mars using hyperspectral sensors

Mars has been surprising us with surfacial expressions of tens of kilometres long river-like channels, dust devils and dunes, deep canyon, tallest and largest volcanoes, large impact basins, and mysterious polar-layered deposits over its surface. A lot has been revealed regarding the origin and evolution of such intriguing surface features, though a lot more has to be explored and understood before achieving a planet-wide perception. One of the ways through which many such Martian mysteries have been deciphered is scanning the surface widely using electromagnetic spectrum at a fine spatial and spectral resolution. However, such a practice has never been easy for Mars, as unlike the Moon, which is an airless body, due to the presence of CO_2 in the atmosphere and minor influence of dust and aerosols, the spectral data acquired from instruments onboard Mars orbiters need corrections for intervening atmosphere. Many atmospheric correction algorithms (viz. DISORT, volcano-scan algorithm, surface–atmosphere separation algorithms, and atmospheric opacity retrieval algorithm) have been developed to correct the acquired data before utilizing them to characterize absorption features of surface materials[84,85].

Clues about the prevailing environmental conditions (alkaline/acidic, oxidizing/reducing) and implications for understanding the temporal evolution of Martian surface
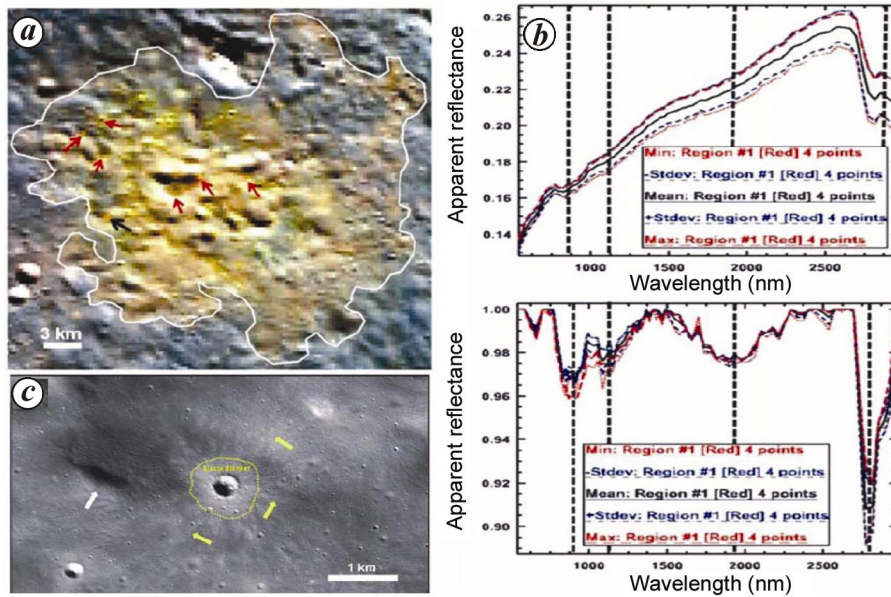
Figure 3. *a*, M³ FCC (R = 0.93 µm, G = 2.0 µm and B = 2.8 µm) of Compton–Belkovich Volcanic Complex with arrow indicating orange pixels that correspond to unusual spectra as shown in (*b*). *b*, Normal and continuum-removed reflectance spectra of orange pixels in (*a*) showing weak absorption features near ~890, 1089 and 1898 nm in association with a strong OH/H₂O feature at 2800 nm. Black dashed lines represent approximate locations of the absorption features. *c*, High-resolution LROC–NAC image of orange pixels marked by black arrow in (*a*) showing a small fresh crater with prominent ejecta rays (marked by yellow arrows) and ejecta blanket demarcated by yellow dotted circle. White arrow indicates a small dome situated to the left of the small ray crater.

could also be established using mineralogical information derived from hyperspectral data. It has been inferred that the southern highland of Mars is mostly unaltered, preserving the old crustal materials showing diversified character of the silicate minerals and hydrous silicate minerals found at numerous outcrops[7]. The northern lowland on the other hand, is resurfaced by thick cover of volcanic and detrital sediments, restricting in deciphering the composition of the underlying ancient crust[86]. Recent observations have outlined evidences for multiple glacial events across many regions in the northern lowland during the late Amazonian[87].

Mars possesses vast similarities to our planet Earth in terms of diversity of minerals detected on its surface. These include silicates, hydrous silicates, carbonates, phyllosilicates and oxides (hematite, limonite), which have been identified by orbital data acquired from various missions such as: Mars Global Surveyor (MGS)-Thermal Emission Spectrometer (TES)[6], Mars Odyssey-Thermal Emission Imaging Systems (THEMIS)[88], Mars Express (MEx)-Observatoire pour la Minéralogie, l'Eau, la Glace et l'Activité (OMEGA)[11], and Mars Reconnaissance Orbiter (MRO)-Compact Reconnaissance Infrared Spectrometer for Mars (CRISM)[89]. From a combined analysis of datasets from these missions, multiple formation scenarios have been suggested for the presence of aqueous minerals detected on the surface of Mars. These includes near-surface weathering, subsurface hydrothermal altera-

tion[90], ice–meltwater or groundwater-assisted weathering[91] and impact cratering.

From the coordinated observations of MEx-OMEGA and MRO-CRISM, a handful of results have been obtained that significantly updated our knowledge on (i) alteration extents of basaltic crust, (ii) evolution and formation of geochemical reservoirs, (iii) composition of Martian mantle and crust, and (iv) evolution of Mars volcanism[92]. Hyperspectral studies are thus able to supply information on altered mineralogy of Mars and provide a geological link between morphology and mineralogy, which allows us to know about the past and present evolutionary histories of Mars.

Hyperspectral imaging of other planetary bodies

Saturn's rings form the largest and brightest ring system and are known to be made of water ice, on the basis of telescopic infrared observations in the late 1970s (ref. 93). After the Voyager encounter with Saturn, the complex composition of rings has received attention which has paved the way for further studies. The composition of Saturn's rings has been studied in detail using the hyperspectral VIMS onboard the Cassini mission. The VIMS instrument consists of two co-aligned imaging spectrometers, VIMS-V and VIMS-IR, providing hyperspectral data in the spectral range 0.35–1.05 and 0.885–5.1 µm respectively[94]. The VIMS instrument is providing data

continuously even after ten years of launch of the Cassini mission. The major satellites of Saturn–Mimas, Enceladus, Tethys, Dione, Rhea, Hyperion, Iapetus and Phobe are predominantly icy objects, whereas the reflectance spectra of these objects in the visible range indicate the presence of colouring agent on all surfaces. Iapetus is known for its differential albedo contrast of two hemispheres, light on one side due to the presence of H_2O ice and dark on the opposite. The first analysis of VIMS spectral data led to the discovery of CO_2 from Iapetus[95]. Further studies related to the composition of low albedo material of Iapetu have shown the presence of both aromatic and aliphatic hydrocarbons[96]. The origin of the material on Iapetus was explained as a possible combination of in-falling dust and endogenic material, which is common in composition of other satellites and the rings.

Asteroids represent a diverse suite of objects that provide important insights into the evolution of nascent early solar system. Studying the mineralogical aspects of asteroids can provide an understanding about the conditions, chemical properties and processes in the early solar system. Vesta is the third largest among the main belt asteroids and being the most fascinating, has been studied to a greater extent. Compositional studies of asteroids were started with Vesta in 1970. The results suggest that it is a differentiated body having a basaltic crust exposed in a huge impact crater indicative of volcanic and/or plutonic processes[97]. Another important reason which makes the study of Vesta significant is the laboratory analysis of reflectance spectra of meteorite samples with suggested genetic link between the Howardite–Eucrite–Diogenite suite of meteorites and Vesta itself[98,99]. Till date no hyperspectral sensor has imaged any asteroid. However, multispectral sensors on-board Dawn Mission, which is a part of NASA's Discovery Program launched in September 2007, have been the first mission for geological studies of asteroid Vesta.

1. Hartmann, W. K., *Moons and Planets*, Wadsworth Publishing Company, 4th edn, 1999.
2. Srivastava, N., Hyperspectral remote sensing in planetary exploration. In *Hyperspectral Remote Sensing and Spectral Signature Applications* (eds Rajendran, S. *et al.*), New India Publishing Agency, 2009, pp. 55–65.
3. Burns, R. G., *Mineralogical Applications of Crystal Field Theory*, Cambridge University Press, New York, 1970.
4. Cloutis, E. A., Pyroxene reflectance spectra: minor absorption bands and effects of elemental substitutions. *J. Geophys. Res.*, 2002, **107**, 6-1–6-12.
5. Schade, U., Wäsch, R. and Moroz, L., Near-infrared reflectance spectroscopy of Ca-rich clinopyroxenes and prospects for remote spectral characterization of planetary surfaces. *Icarus*, 2004, **168**, 80–92.
6. Banfield, J. L., Hamilton, V. E. and Christensen, P. R., A global view of martian surface compositions from MGS-TES. *Science*, 2000, **287**, 1626–1630.
7. Banfield, J. L., Global mineral distributions on Mars. *J. Geophys. Res.*, 2002, **107**, doi: 10.1029/2001JE001510.

8. Pieters, C. M., Mare basalt types on the front side of the Moon: a summary of spectral reflectance data. In Proceedings of the 9th Lunar and Planetary Science Conference, Houston, Texas, 1978, pp. 2825–2849.
9. McCord, T. B. and Clark, R. N., The Mercury soil: presence of Fe^{2+}. *J. Geophys. Res.*, 1979, **84**, 7664–7668.
10. McCord, T. B., Adams, J. B. and Johnson, T. V., Asteroid Vesta: spectral reflectivity and compositional implications. *Science*, 1970, **168**, 1445–1447.
11. Mustard, J. F. *et al.*, Olivine and pyroxene diversity in the crust of Mars. *Science*, 2005, **307**, 1594–1597.
12. Mustard, J. F. *et al.*, Mineralogy of the Nili Fossae region with OMEGA/Mars Express data: ancient impact melt in the Isidis Basin and implications for the transition from Noachian to Hesperian. *J. Geophys. Res.*, 2007, **112**, E08S03; doi: 10.1029/2006JE002834.
13. Chauhan, P. *et al.*, Integrated analysis of topographically high mafic exposures at Apollo-17 landing site using data from imaging sensors on Chandrayaan-1. In Lunar and Planetary Science Conference, The Woodland, Texas, 2010, vol. 41, abstr. 1533.
14. Bhattacharya, S., Chauhan, P., Rajawat, A. S. and Kiran Kumar, A. S., Lithological mapping of central part of Moscoviense using Chandrayaan-1 hyperspectral Imager (HySI) data. *Icarus*, 2011, **212**, 470–490, doi: 10.1016/j.icarus.2011.02.006.
15. Kaur, P., Bhattacharya, S., Chauhan, P., Ajai and Kiran Kumar, A. S., Mineralogy of Mare Serenitatis on the near side of the Moon based on Chandrayaan-1 Moon Mineralogy Mapper (M^3) observations. *Icarus*, 2013, **222**, 137–148.
16. Varatharajan, I., Srivastava, N. and Murty, S. V. S., Mineralogy of young lunar mare basalts: Assessment of temporal and spatial heterogeneity using M^3 data from Chandrayaan-1, *Icarus*, 2014, doi: 10.1016/j.icarus.2014.03.045.
17. Kusuma, K. N., Sebastian, N. and Murty, S. V. S., Geochemical and mineralogical analysis of Gruithuisen region on Moon using M^3 and DIVINER images. *Planet. Space Sci.*, 2012, **67**, 46–56.
18. Chauhan, P., Kaur, P., Srivastava, N., Bhattacharya, S., Ajai, Kiran Kumar, A. S. and Goswami, J. N., Compositional and morphological analysis of high resolution remote sensing data over central peak of Tycho crater on the Moon: implications for understanding lunar interior. *Curr. Sci.*, 2012, **102**(7), 1041–1046.
19. Isaacson, P. J. *et al.*, Remote compositional analysis of lunar olivine-rich lithologies with Moon Mineralogical Mapper (M^3) spectra. *J. Geophys. Res.*, 2011, **116**, E00G11.
20. Staid, M. I. *et al.*, The mineralogy of late stage lunar volcanism as observed by the Moon Mineralogical Mapper on Chandrayaan-1. *J. Geophys. Res.*, 2011, **116**, E00G10.
21. Filacchione, G. *et al.*, Cassini-VMS observations of Saturn's main rings: I. Spectral properties and temperature radial profiles variability with phase angle and elevation. *Icarus*, 2014, **214**, 45–65.
22. Clark, R. N. *et al.*, The surface composition of Iapetus: mapping results from Cassini VIMS. *Icarus*, 2012, **218**, 831–860.
23. Bishop, J. L. *et al.*, Phyllosilicate diversity and past aqueous activity revealed at Mawrth Vallis, Mars. *Science*, 2008, **321**, 830; doi: 10.1126/science.1159699.
24. Mangfold, N. *et al.*, Mineralogy of the Nili Fossae region with OMEGA/Mars Express data: 2. Aqueous alteration of the crust. *J. Geophys. Res.*, 2007, **112**, E08S04; doi: 10.1029/2006JE002835.
25. Surkov, Y. A. *et al.*, Determination of the elemental composition of rocks on Venus by Venera 13 and Venera 14 (Preliminary results). *J. Geophys. Res.* (*Suppl.*), 1983, **88**, A481–A492.
26. Basaltic Volcanism Study Project, *Basaltic Volcanism on the Terrestrial Planets*, Pergamon, New York, 1981.
27. Singer, R. B., Miller, J. S., Wells, K. W. and Bus, E. S., Visible and near-IR spectral imaging of Mars during the 1988 opposition. In Lunar and Planetary Science Conference, Houston, Texas, 1990, vol. 21, pp. 1164–1165.

28. Cruikshank, D. P., Tholen, D. J., Hartmann, W. K., Bell, J. F. and Brown, R. H., Three basaltic Earth-approaching asteroids and the source of basaltic meteorites. *Icarus*, 1991, **89**, 1–13.

29. Wood, C. A. and Ashwal, L. D., SNC meteorites: igneous rocks from Mars? In Proceedings of Lunar and Planetary Science Conference, Houston, Texas, 1981, vol. 12, pp. 1359–1375.

30. Clark Jr, S. P., Absorption spectra of some silicates in the visible and near infrared. *Am. Mineral.*, 1957, **42**, 732–742.

31. Clark, R. N., King, T. V. V., Klejwa, M., Swayze, G. A. and Vergo, N., High spectral resolution reflectance spectroscopy of minerals. *J. Geophys. Res.*, 1990, **95**, 12653–12680.

32. Pieters, C. M. *et al.*, Space weathering on airless bodies: resolving a mystery with lunar samples. *Meteorol. Planet. Sci.*, 2000, **35**, 1101–1107.

33. Noble, S., Pieters, C. and Keller, L. P., An experimental approach to understanding the optical effects of space weathering. *Icarus*, 2007, **192**, 629–642.

34. Viviano-Beck, C. E. *et al.*, Revised CRISM spectral parameters and summary products based on the currently detected mineral diversity on Mars. *J. Geophys. Res. Planets*, 2014, **119**, 1403–1431.

35. Pieters, C. M. and McCord, T. M., Characterization of lunar mare basalt types. I. A remote sensing study using reflection spectroscopy of surface soils. In Proceedings of the 7th Lunar Science Conference, Houston, Texas, 1976, pp. 2677–2690.

36. Johnson, T. V., Saunders, R. S., Matson, D. L. and Mosher, J. A., A TiO_2 abundance map for the northern maria. In Proceedings of the 8th Lunar Planetary Science Conference, Houston, Texas, 1977, pp. 1029–1036.

37. Adams, J. B. *et al.*, Remote sensing of basalts in the Solar System. In *Basaltic Volcanism on the Terrestrial Planets* (Basaltic Volcanism Study Project), Pergamon, New York, 1981, pp. 438–490.

38. Robinson, M. S., Hawke, B. R., Lucey, P. G. and Smith, G. A., Mariner 10 multispectral images of the eastern limb and farside of the Moon. *J. Geophys. Res.*, 1992, **97**, 18265–18274.

39. Greeley, R. *et al.*, Galileo observations of Lunar Maria and related deposits. *J. Geophys. Res.*, 1993, **98**, 17183–17205.

40. Williams, D. A., Greeley, R., Neukum, G. and Wagner, R., Multispectral studies of selected crater- and basin-filling lunar maria from Galileo Earth–Moon encounter. In Lunar and Planetary Science Conference, Houston, Texas, 1993, vol. 24, pp. 1521–1522.

41. Nozette, S. *et al.*, The Clementine Mission to the Moon – scientific overview. *Science*, 1994, **266**, 1835–1839.

42. Pieters, C. M., Compositional diversity and stratigraphy of the lunar crust derived from reflectance spectroscopy. In *Remote Geochemical Analysis: Elemental and Mineralogical Composition*, Cambridge University Press, Cambridge, UK, 1993, pp. 309–339.

43. McEwen, A. S. and Robinson, M. S., Mapping of the Moon by Clementine. *Adv. Space Res.*, 1997, **19**, 1523–1533.

44. Tompkins, S. and Pieters, C. M., Mineralogy of the lunar crust: results from Clementine. *Meteor. Planet. Sci.*, 1999, **34**, 25–41.

45. Isaacson, P. J. and Pieters, C. M., Northern Imbrium Noritic anomaly. *J. Geophys. Res.*, 2009, **114**, E09007.

46. Lucey, P., Taylor, G. and Malaret, E., Abundance and distribution of iron on the Moon. *Science*, 1995, **268**, 1150–1153.

47. Blewett, D. T., Lucey, P. G., Hawke, B. R. and Jolliff, B. L., Clementine images of the lunar sample-return stations: refinement of FeO and TiO_2 mapping techniques. *J. Geophys. Res.*, 1997, **102**, 16319–16325.

48. Lucey, P. G., Blewett, D. T., Taylor, G. J. and Hawke, B. R., Imaging of the lunar surface maturity. *J. Geophys. Res.*, 2000, **105**, 20377–20386.

49. Srivastava, N., Geochemical estimates of iron and titanium for the central peaks of lunar crater. In Lunar and Planetary Science Conference, Houston, 2007, vol. 38, abstr. 1338.

50. Srivastava, N., Titanium estimates of the central peaks of lunar craters: implications for sub surface lithology of moon. *Adv. Space Res.*, 2008, **42**, 281–284.

51. Lawrence, D. J. *et al.*, Iron abundances on the lunar surface as measured by the lunar prospector gamma-ray and neutron spectrometers. *J. Geophys. Res.*, 2002, **107**(E12), 5130; doi: 10.1029/2001JE001530.

52. Kramer, G. Y., Jolliff, B. L. and Neal, C. R., Distinguishing high-alumina UV–VIS and Lunar Prospector GRS data: Mare Moscoviense and Mare Nectaris. *J. Geophys. Res.*, 2008, **113**, E01002; doi: 10.1029/2006JE002860.

53. Garrick-Bethell, I. and Zuber, M. T., An indigenous origin for the South Pole Aitken basin thorium anamoly. *Geophys. Res. Lett.*, 2005, **32**, L13203; doi: 10.1029/2005GL023142.

54. Lawrence, S. J. *et al.*, Composition and origin of the Dewar geochemical anomaly. *J. Geophys. Res.*, 2008, **113**, E02001; doi: 10.1029/2007JE002904.

55. Kato, M. *et al.*, The Kaguya mission overview. *Space Sci. Rev.*, 2010, **154**, 3–19.

56. Haruyama, J. *et al.*, Global lunar-surface mapping experiment using the lunar imager/spectrometer on SELENE. *Earth Planets Space*, 2008, **60**, 243–255.

57. Goswami, J. N. and Annadurai, M., An overview of the Chandrayaan-1 mission. *Curr. Sci.*, 2009, **96**, 486–491.

58. Kumar, A. *et al.*, Hyper spectral imager for lunar mineral mapping in visible and near infrared band. *Curr. Sci.*, 2009, **96**, 496.

59. Mall, U. *et al.*, Near infrared spectrometer SIR-2 on Chandrayaan-1. *Curr. Sci.*, 2009, **96**, 506–511.

60. Boardman, J. W. *et al.*, Measuring moonlight: an overview of the spatial properties, lunar coverage, selenolocation and related level 1b products of the Moon Mineralogical Mapper. *J. Geophys. Res.*, 2011, **116**, E00G14.

61. Warren, P. H., Lunar anorthosites and the magma–ocean plagioclase-flotation hypotheses: importance of FeO enrichment in the parent magma. *Am. Mineral.*, 1990, **75**, 46–58.

62. Matsunaga, T. *et al.*, Discoveries on the lithology of lunar crater central peaks by SELENE Spectral Profiler. *Geophys. Res. Lett.*, 2008, **35**, L23201; doi: 10.1029/2008GL035868.

63. Pieters, C. M. and Tompkins, S., Tsiolkovsky crater: a window into crustal processes on the lunar far side. *J. Geophys. Res.*, 1999, **104**, 21935–21494.

64. Yamamoto, S. *et al.*, Possible mantle origin of olivine around lunar impact basins detected by SELENE. *Nature Geosci. Lett.*, 2010, doi: 10.1038/ngeo897.

65. Pieters, C. M. *et al.*, Mg-spinel lithology: a new rock type on the lunar farside. *J. Geophys. Res.*, 2011, **116**, E00G08.

66. Dhingra, D. *et al.*, Compositional diversity at Theophilus Crater: understanding the geological context of Mg-spinel bearing central peaks. *Geophys. Res. Lett.*, 2011, **38**, L11201.

67. Lal, D., Detection of Mg spinel lithologies on central peak of crater Theophilus using Moon Mineralogy Mapper (M^3) data from Chandrayaan-1. *J. Earth Syst. Sci.*, 2012, **121**, 847–853.

68. Kaur, P., Chauhan, P., Bhattacharya, S., Ajai and Kiran Kumar, A. S., Compositional diversity at Tycho crater: Mg-spinel exposures detected from Moon Mineralogical Mapper (M^3) data. In Lunar and Planetary Science Conference, Texas, 2012, vol. 43, abstr. 1434.

69. Kaur, P., Chauhan, P. and Ajai, Detection of Mg-spinel exposures from the anorthositic terrain surrounding Mare Ingenii on the far side of the Moon. In Lunar and Planetary Science Conference, Texas, 2013, vol. 44, abstr. 1547.

70. Srivastava, N. and Gupta, R. P., Compositional diversity inside Lowell crater, Orientale Basin: evidences for extensive spinel rich deposits. In Conference on Lunar Highland Crust, 2012, vol. 2, abstr. 9016.

71. Kaur, P. and Chauhan, P., Detection of spinels exposures from some near side locations of the Moon. In Lunar and Planetary Science Conference, Texas, 2014, vol. 45, abstr. 2059.

72. Kaur, P., Chauhan, P. and Ajai, Exposures of Mg-spinel on an evolved silicic lithology Hansteen Alpha on the moon. In Lunar

and Planetary Science Conference, Texas, 2013, vol. 44, abstr. 1348.

73. Bhattacharya, S. *et al.*, Discovery of orthopyroxene–olivine–spinel assemblage from the lunar nearside using Chadrayaan-1 Moon Mineralogy Mapper data. *Curr. Sci.*, 2012, **102**, 21–23.

74. Srivastava, N. and Gupta, R. P., Spatial distribution of spinel in the Orientale basin: new insights from M^3 data. In Lunar and Planetary Science Conference, Texas, 2013, vol. 44, abstr. 1509.

75. Bhattacharya, S., Chauhan, P., Rajawat, A. S., Ajai and Kiran Kumar, A. S., Lithological mapping of central part of Mare Moscoviense using Chandrayaan-1 Hyperspectral Imager (HySI) data. *Icarus*, 2011, **212**, 470–479.

76. King, T. V. and Ridley, W. I., Relation of the spectroscopic reflectance of olivine to mineral chemistry and some remote sensing implications. *J. Geophys. Res.*, 1987, **92**, 11457–11469.

77. Mustard, J. F. *et al.*, Compositional diversity and geologic insights of the Aristarchus crater from Moon Mineralogy Mapper data. *J. Geophys. Res.*, 2011, **116**, E00G10.

78. Srivastava, N., Kumar, D. and Gupta, R. P., Young viscous flows in the Lowell crater of Orientale basin, Moon: impact melts or volcanic eruptions? *Planet. Space Sci.*, 2013, **87**, 37–45.

79. Gupta, R. P., Srivastava, N. and Tiwari, R. K., Evidences of relatively fresh volcanic flows on the Moon. *Curr. Sci.*, 2014, **107**(3), 454–460.

80. Pieters, C. M. *et al.*, Character and spatial distribution of OH/H_2O on the surface of the Moon seen by Chandrayaan-1. *Science*, 2009, **326**; doi: 10.1126/science.1178658.

81. Bhattacharya, S., Saran, S., Dagar, A., Chauhan, P., Chauhan, M., Ajai and Kiran Kumar, A. S., Endogenic water on the Moon associated with non-mare silicic volcanism: implications for hydrated lunar interior. *Curr. Sci.*, 2013, **150**, 685–691.

82. Chauhan, P., Kaur, P., Bhattacharya, S., Dagar, A. and Kiran Kumar, A. S., Detection of OH/H_2O on the central peak of Jackson crater from Moon Mineralogical Mapper (M^3) data onboard Chandrayaan-1. In Lunar and Planetary Science Conference, Texas, 2014, vol. 45, abstr. 2072.

83. Klima, R. L., Cahill, J., Hagerty, J. and Lawrence, D., Remote detection of magmatic water in Bullialdus Crater on the Moon. *Nature Geosci.*, 2013, **6**, 737–741; doi: 10.1038/ngeo1909.

84. Smith, M. D., Bandfield, J. L. and Christensen, P. R., Separation of surface and atmospheric spectral features in Mars Global Surveyor Thermal Emission Spectrometer (TES) spectra. *J. Geophys. Res.*, 2000, **105**, 9589–9608.

85. McGuire, P. C. *et al.*, An improvement to the volcano-scan algorithm for atmospheric correction of CRISM and OMEGA spectral data. *Planet. Space Sci.*, 2009, **57**, 809–815.

86. Baker, V. R. *et al.*, Ancient oceans, ice sheets and the hydrological cycle on Mars. *Nature*, 1991, **352**, 589–594.

87. Sinha, R. K. and Murty, S. V. S., Geomorphic signatures of glacial activity in the Alba Patera volcanic province: implications for recent frost accumulation on Mars. *J. Geophys. Res.*, 2013, **118**, 1609–1631.

88. Christensen, P. R. *et al.*, Morphology and composition of the surface of Mars: Mars Odyssey THEMIS results. *Science*, 2003, **300**, 2056–2061.

89. Carter, J., Poulet, F., Bibring, J.-P., Mangold, N. and Murchie, S., Hydrous minerals on Mars as seen by the CRISM and OMEGA imaging spectrometers: updated global view. *J. Geophys. Res. Planets*, 2013, **118**, 831–858.

90. Jain, N., Bhattacharya, S. and Chauhan, P., Aqueous minerals from Arsia Chasmata of Arsia Mons, Tharsis region: implications for aqueous alteration processes on Mars. In Lunar and Planetary Science Conference, 2014, vol. 45, abstr. 1826.

91. Jain, N., Bhattacharya, S., Chauhan, P. and Ajai, Study of phyllosilicates and carbonates from the Capri Chasma region of Valles Marineris on Mars based on Mars Reconnaissance Orbiter-Compact Reconnaissance Imaging Spectrometer For Mars (MRO-CRISM) observations. In Lunar and Planetary Science Conference, Texas, 2014, vol. 45, abstr. 1821.

92. Sinha, R. K. and Murty, S. V. S., Nature and distribution of olivine in Moreux crater in northern mid-latitude of Mars. In Lunar and Planetary Science Conference, 2013, vol. 44, abstr. 1179.

93. Kuiper, G. P., Cruikshank, D. P. and Fink, U., The composition of Saturn's rings. *Sky Telescope*, 1970, **39**, 14.

94. Brown, R. H. *et al.*, The Cassini Visual and Infrared Mapping Spectrometer (VIMS) investigation. *Space Sci. Rev.*, 2004, **115**, 111–168.

95. Buratti, B. J. *et al.*, Cassini Visual and Infrared Mapping Spectrometer observations of Iapetus: detection of CO_2. *Astrophys. J.*, 2005, **622**, L149–L152.

96. Cruikshank, D. P. *et al.* and the VIMS Team, Hydrocarbons on Saturn's satellites Iapetus and Phoebe. *Icarus*, 2008, **193**, 334–343.

97. McCord, T. B., Adams, J. B. and Johnson, T. V., Asteroid Vesta: spectral reflectivity and compositional implications. *Science*, 1970, **168**, 1445–1447.

98. Burbine, T. H. *et al.*, Vesta, vestoids, and the howardites, eucrite, diogenite group: relationships and the origin of spectral differences. *Meteorit. Planet. Sci.*, 2001, **36**, 761–781.

99. McSween, H. Y., Mittlefehldt, D. W., Beck, A. W., Mayne, R. G. and McCoy, T. J., HED meteorites and their relationship to the geology of Vesta and the Dawn mission. *Space Sci. Rev.*, 2011, **163**, 141–174.